This article is a non-peer reviewed preprint, it was submitted to the journal Scientific Reports on April 5th 2023.

Global multi-hazard risk assessment in a changing climate

Zélie Stalhandske[1,2*+], Carmen B. Steinmann[1,2+], Simona Meiler[1,2], Inga J. Sauer[1,3], Thomas Vogt[3], David N. Bresch[1,2], and Chahan M. Kropf[1,2]

[1]Institute for Environmental Decisions, ETH Zurich, Zurich, 8092, Switzerland
[2]Federal Office of Meteorology and Climatology MeteoSwiss, Zurich-Airport, 8058, Switzerland
[3]Potsdam Institute for Climate Impact Research, Potsdam, 14473, Germany
[*]zelie.stalhandske@usys.ethz.ch
[+]these authors contributed equally to this work

ABSTRACT

Natural hazards pose significant risks to people and assets in many regions of the world. Quantifying associated risks is crucial for many applications such as adaptation option appraisal and insurance pricing. However, traditional risk assessment approaches have focused on the impacts of single hazards, ignoring the effects of multi-hazard risks and potentially leading to underestimations or overestimations of risks. In this work, we present a framework for modelling multi-hazard risks globally in a consistent way, considering hazards, exposures, vulnerabilities, and assumptions on recovery. We illustrate the approach using river floods and tropical cyclones impacting people and physical assets on a global scale in a changing climate. To ensure physical consistency, we combine single hazard models that were driven by the same climate model realizations. Our results show that incorporating common physical drivers and recovery considerably alters the multi-hazard risk. This framework is implemented in the open-source climate risk assessment platform CLIMADA and can be applied to various hazards and exposures, providing a more comprehensive approach to risk management than conventional methods.

Introduction

Climate change is affecting natural and socio-economic systems in all parts of the world. In this context, the Intergovernmental Panel on Climate Change (IPCC) has defined climate risks as arising from the dynamic interactions between climate-related hazards and the exposure and vulnerability of affected human and ecological systems[1]. This definition has been taken up by many studies that typically focus on a single hazard affecting an exposure[2]. However, since multiple hazards can challenge these systems, focusing on a single hazard can result in an incomplete assessment of the risk. Combining risks from multiple single hazards by assuming them to be independent is a first step towards a more comprehensive risk assessment. This type of risk assessment is defined by the European Commission as multi-layer single-hazard risk assessment[3]. This allows to compute a shared exceedance probability of losses using individual risk estimates[4]. However, this approach neglects the effects of temporal sequence and co-occurrence of events on risk. Therefore, there have been international calls for more attention to multi-hazards and multi-risks[5] and for harmonization of related definitions[3,6,7].

The European Commission defines multi-hazard risk as the assessment of the interactions between single hazards, in contrast to multi-layer single-hazards[3]. These interactions are classified into five groups based on Gill and Malamud's work in 2014 and 2016, which include triggering, increased probability, decreased probability, coincidence, and catalysis/impedance relationships[8,9]. Based on these hazard interactions, the resulting risk assessment is considered as multi-hazard risk. Furthermore, a more comprehensive approach would involve including dynamic vulnerabilities, resulting in a multi-risk assessment.

In parallel, the concept of compound events has emerged in recent years in weather and climate science. In that context, compound events are defined as the combination of multiple drivers and/or hazards that contribute to societal or environmental risk[10]. The term compound has typically been applied to describe events co-occurring over meteorological timescales (hours to weeks), and to express the resulting intensification of the negative aspects[11]. Complementary, Hillier et al. (2020) propose the definition of compound risks to include risks that compound on extended time-frames which are more relevant for decision making; and whose compounding can also lead to decreased risks[11]. This definition recognizes that private and public organizations face an increasing global exposure to natural hazards and that methods that account for atmospheric connections between hazards (tele-connections) are necessary to manage and mitigate risks. By accounting for these connections at the relevant time and spatial scale for a given decision-making process, a more accurate evaluation of risks can be provided, preventing overestimation and underestimation, which can both be problematic[11].

When transitioning from analyzing single hazards to multiple hazards, it is necessary to establish a common timescale to consider how these hazards interact. As one progresses to examining the impacts and risks of these hazards, a choice must be made regarding how to model the exposures and vulnerabilities on the defined timescale. Merely assuming static exposures and vulnerabilities can result in inconsistencies. For example, consider a house that is destroyed by both a tornado and a wildfire in the same week. If this house is counted as destroyed twice, it would be inaccurate as it cannot be reconstructed within a week. In other words, when assessing compound risks of multiple hazards, it is essential to consider the assumptions made about the recovery of the exposures and changes in their vulnerabilities[3,12].

In this study, we provide a framework for assessing multi-hazard risks under different climate conditions. We build upon the compound risk definition provided by Hillier et al. (2020)[11] to investigate spatially compounding risk occurring in the same time window (e.g., a day, a season, or a year) on a global scale; and spatio-temporally compounding risk occurring at the same location in the same time window. We focus on global river floods (RF) and tropical cyclones (TC), the two hazards currently affecting the largest number of people and causing the highest damage to physical assets[13]. We use TC and RF footprints from the Inter-Sectoral Impact Model Intercomparison Project ISIMIP models[14] that take the same set of Global Climate Models (GCMs) as input. This basis of common climatic inputs allows combining hazard (RF and TC) realisations that share physical drivers, even if they were modelled independently from one another. In order to showcase their effects on different exposure types, we assess the impacts of both hazards on population and economic assets. We chose to report annual risk metrics, as they are of high relevance for decision-making[15]. With the IPCC showing that human activities are responsible for a global warming of about 1.1 °C since pre-industrial levels (1850-1900)[16], we choose model simulations based on GCM runs at 1 °C warming level as representation of today's world. Moreover, with climate change exacerbating the frequency and intensity of natural hazards[16], we additionally assess the risk in a 2 °C world. We finally discuss the requirements for advancing towards a complete multi-risk assessment. All methods are implemented in the open-source climate-risk assessment platform CLIMADA[17], which allows the analysis of probabilistic event sets under present and future climatic conditions. A multitude of hazards are represented in CLIMADA and can be considered in future work on multi-hazard risk. This study is the first to our knowledge to assess multi-hazard risks on an event basis at a global scale in a consistent fashion across GCMs.

Results

To assess spatially compounding and spatio-temporally compounding multi-hazard impacts, we combine single-hazard impacts with a four-step process. The single-hazard sets contain individual events. The impact of each event is calculated by combining the three components hazard, exposure and vulnerability. The vulnerability of the given exposure is described by an impact function which constitutes the relationship of the respective hazard intensity and the caused impact[17]. Event impacts are computed separately for each exposure type at every exposure location (see Methods for more details on the single hazard risk calculation). Second, we define a time period of interest, e.g. one calendar year y. In order to compute annual impacts for one hazard we sum all event impacts of the respective hazard occurring within one year at each exposure location. Here one has to make an assumption about the recovery of the exposures between multiple events during the time period. The simplest case assumes no recovery which can be modelled by capping the annual impact at each location at the total value of the exposure at said location. When working with GCMs, each year y has a realisation driven by each GCM, resulting in the annual impact for hazard h, GCM model g in year y at location k given by

$$I_{h,k}^{y,g} = \min\left(E_k, \sum_{\varepsilon=1}^{L_h^{y,g}} I_{\varepsilon,h,k}\right) \tag{1}$$

where E_k is the value of the exposure at location k and $L_h^{y,g}$ the number of events ε in year y for GCM g and hazard h. Third, these single-hazard impacts are added among hazards for the respective GCM year; and capped again. The spatially compounding multi-hazard global annual impact in year y for GCM g is then

$$S^{y,g} = \sum_k \min\left(E_k, \sum_h I_{h,k}^{y,g}\right). \tag{2}$$

By combining single-hazard years driven by the same year of the same GCM, common physical drivers can be maintained when adding impacts. Capping impacts at the exposure value at each point corresponds to assuming that the maximum compounded multi-hazard impact per year cannot exceed the exposure value (i.e., no recovery within a year). Computing these impacts for each year y independently assumes full recovery at the end of each calendar year. In the last step, the spatio-temporally compounding multi-hazard global annual impact for GCM g is obtained by summing the impact of all exposure locations k affected by events of two hazard h in the respective year y:

$$T^{y,g}_{h_i h_j} = \sum_k \begin{cases} \min\left(E_k, \sum_{h=i,j} I^{y,h}_k\right), & \text{if } I^{y,i}_k \geq 0 \text{ and } I^{y,j}_k \geq 0 \\ 0, & \text{otherwise} \end{cases}. \tag{3}$$

When studying three or more hazards, each grouping of hazards would result in a spatio-temporally compounding multi-hazard global annual impact, analogously to Eq. 3. Risk is calculated by multiplying the severity of events (here impacts Eqs. 1 - 3) with their probability of occurrence in the given time period.

In this work, we analyze 5000 years of spatially compounding and spatio-temporally compounding multi-hazard impacts for the global ISIMIP hazards TC and RF affecting the exposures physical assets and affected population. While the impact functions for assets are regional sigmoid curves, people are considered to be affected based on a threshold of 1m flood depth (for RF) and 33m/s wind speed (for TC) (See SI section 4.1). Affected could mean, for example, displaced, injured or experiencing a loss of livelihood. Capping impacts at the exposure value at each point corresponds to assuming that each asset can only be damaged fully once each year or that each person can only be affected once. Finally, this also assumes that both people and assets fully recover at the end of each calendar year. In order to study impacts and risks at different warming levels, we make use of the year $y_{w,g}$ in which a certain GCM g reaches a given warming level w. We extract 10 years before and after $y_{w,g}$ for the warming levels 1 °C, 2 °C and each of the 4 GCMs g. This results in a 21 years time window ($U_{w,h,g}$) per warming level w, hazard h and GCM g. Within each year the ISIMIP hazard sets contain one RF and several TC events. After computing the spatially compounding or spatio-temporally compounding multi-hazard global annual impact (c.f., Eqs. 1 - 3), we disregard the sequence of years within GCMs and use all years U_w belonging to one warming level w for risk computations. Each spatially compounding or spatio-temporally compounding multi-hazard global annual impact has a probability $P = 1/U_w$ to occur in year y, and the resulting risks are then $R^{y,g,w}_S = S^{y,g} \cdot 1/U_w$ and $R^{y,g,w}_T = T^{y,g} \cdot 1/U_w$, respectively.

Impact & risk maps

With the defined spatio-temporally compounding impacts, we study the worldwide distribution of annual co-occurrence of RF and TC, as shown for example years y_1 and y_2 in Fig. 1. These years are chosen to be years were the spatio-temporally compounding impacts reach the value of a one in a hundred year impact (100-yr impact) for the warming level 1.0 °C. This means that on average every hundred years, we would expect this value of exposures affected by both hazards to be reached at that warming level. In the case of assets, this corresponds to the GCM HADGEM2-ES for the year 2012 under RCP6.0. In the case of population this corresponds to the GCM GFDL-ESM2M for the year 2008 under RCP2.6. The distribution is typically heterogeneous, with only few regions worldwide impacted by both TC and RF in these years ($I_{RF,k} > 0$, $I_{TC,k} > 0$), while most impacted regions experience either RF ($I_{RF,k} > 0$, $I_{TC,k} = 0$) or TC ($I_{RF,k} = 0$, $I_{TC,k} > 0$). This is both the case for assets (Fig. 1a), where compounding takes place mostly in East Asia, Central America, and East Africa, and for population (Fig. 1b), where compounding takes place mostly in East Asia and Central America.

Beyond individual years, one can also study common risk metrics such as the average annual impact (AAI), which is often used as a proxy for risk-based insurance premiums. The average annual impact is obtained by averaging the annual impact over all years corresponding to a given warming level. The AAI can be studied for different geographical scales, for example at each exposure point, by country or globally.

Fig. 2 shows exposure points that exceed 1000 dollars (in 2a) and 100 people affected (in 2b) in AAI. When examining the risk of the two hazards on population, we observe that fewer exposure points are affected. This can be attributed to the definition of vulnerability, were we consider 100% impact above the defined thresholds and no impact below. The spatio-temporally compounding scatter points in these maps highlight geographical areas for which adopting a multi-hazard risk or multi-risk framework is most relevant for the two studied hazards. Indeed, the exposures highlighted in purple are commonly affected by spatio-temporally compounding hazards. Recovery, as well as multi-hazard vulnerability may therefore be particularly important for those.

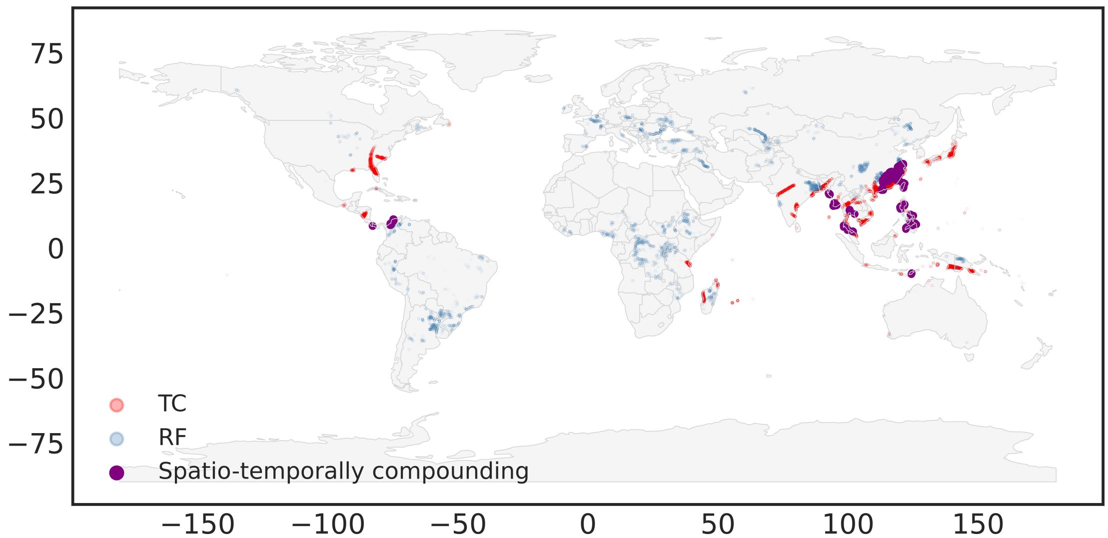

(a) Asset exposures.

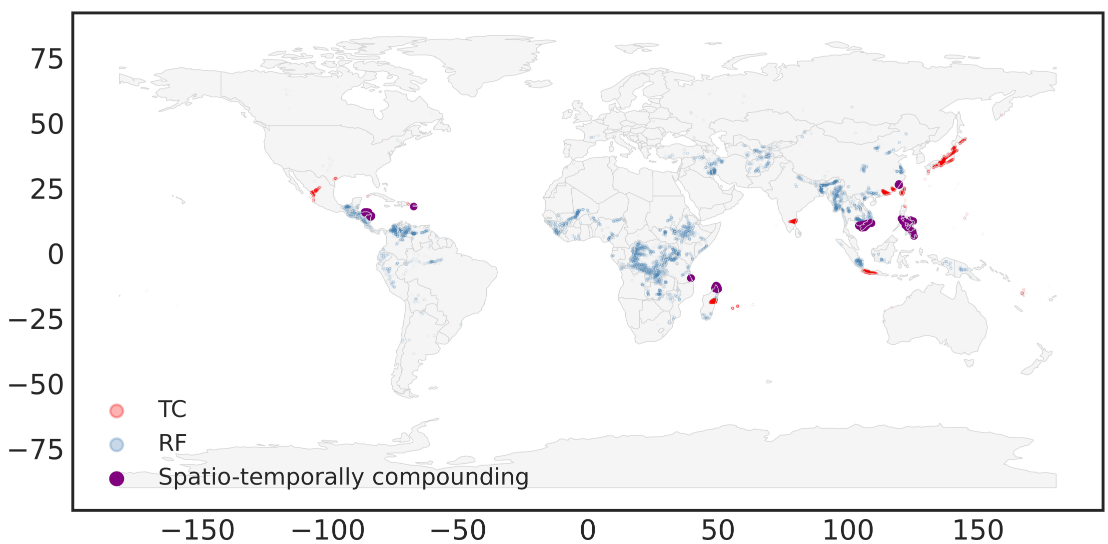

(b) Population exposure.

Figure 1. Illustration of the spatio-temporally compounding impact of TC and RF. Each exposure point is either impacted by TC (red) only, RF (blue) only, both (purple), or neither (grey). The impact is shown for the warming level 1.0 °C for assets (top panel) and population (bottom panel) for a given example year chosen to best illustrate the compounding distribution heterogeneity. Note that the year for a) is different than for b).

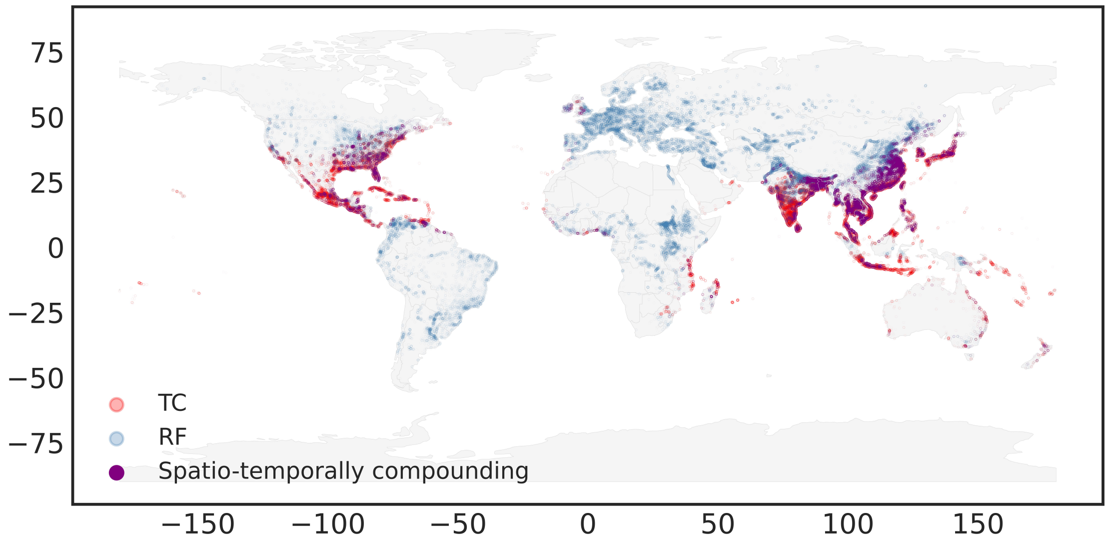

(a) Asset exposure points affected by TC, RF and their compound on average per year

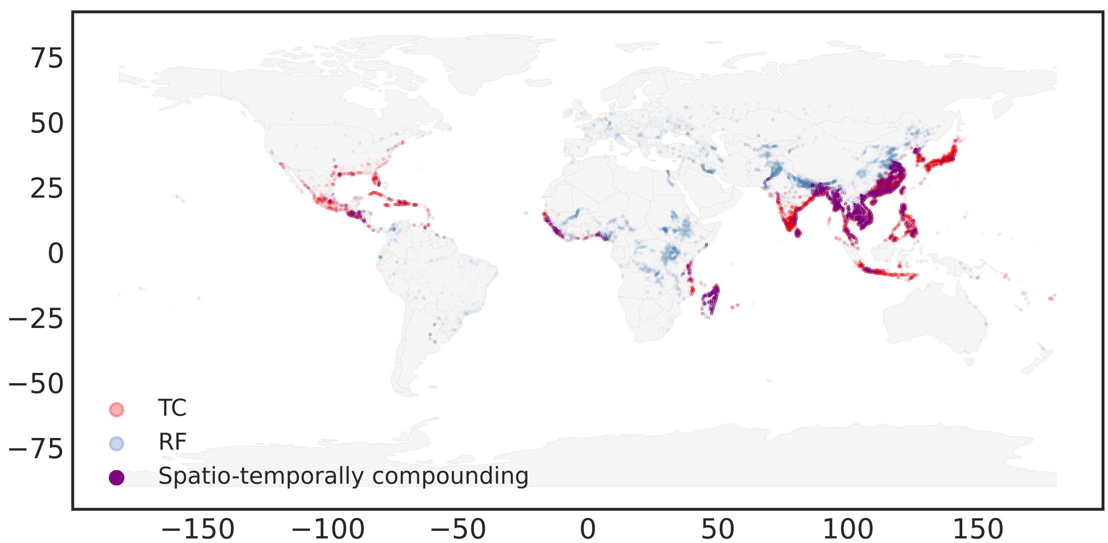

(b) Population exposure points affected by TC, RF and their compound on average per year

Figure 2. Exposure points with at least (a) 1000 dollar damage or (b) at least 100 people affected on average per year from either TC, RF or the spatio-temporally compounding impacts (impacts from both hazard occurring in the same year) at a 1.0 °C warming level.

Impact return period curves of spatially compounding risk

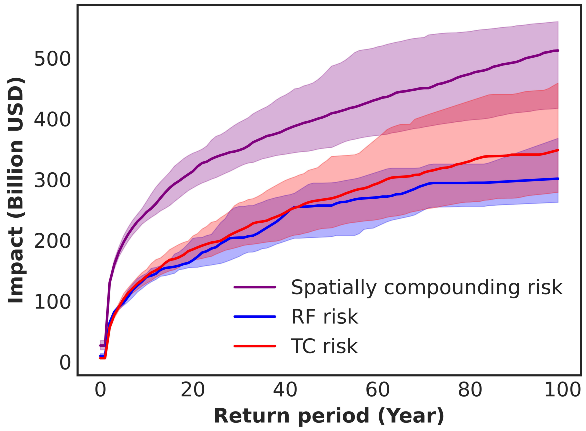

(a) Impact return period curve for assets

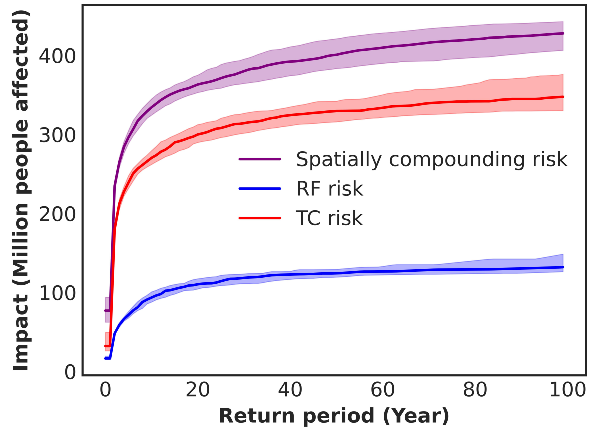

(b) Impact return period curve for population

Figure 3. Impact return period curves of RF, TC and the spatial compounding of both, at 1.0 °C. The shaded area is the 90th confidence interval for 1000 samples of 500 years, while the full lines represent the median of all samples.

An impact return period curve represents an additional valuable risk metric, which describes the probabilistic cumulative distribution of impacts. From this curve, one can for example read the 100-yr impact, which is a useful metric that provides a standardized way of comparing the potential impact of natural hazards for a defined geographical area. It helps to guide risk management and mitigation strategies, and is used as a benchmark for determining insurance premiums and other financial policies related to natural hazards. Fig. 3 displays the impact return period curve for up to 100 years of RF, TC, as well as their spatially compounding risk curve at 1.0 °C of global warming. In the case of assets, both hazards result in similar risk curves, while for population the TC risk is higher than for RF. Additionally, the spread between samples is larger for assets. These differences between population and assets can again be explained by the difference in vulnerability definition. We recall that population vulnerabilities are defined based on a threshold above which people are considered affected, while assets vulnerabilities are defined as regional sigmoid functions.

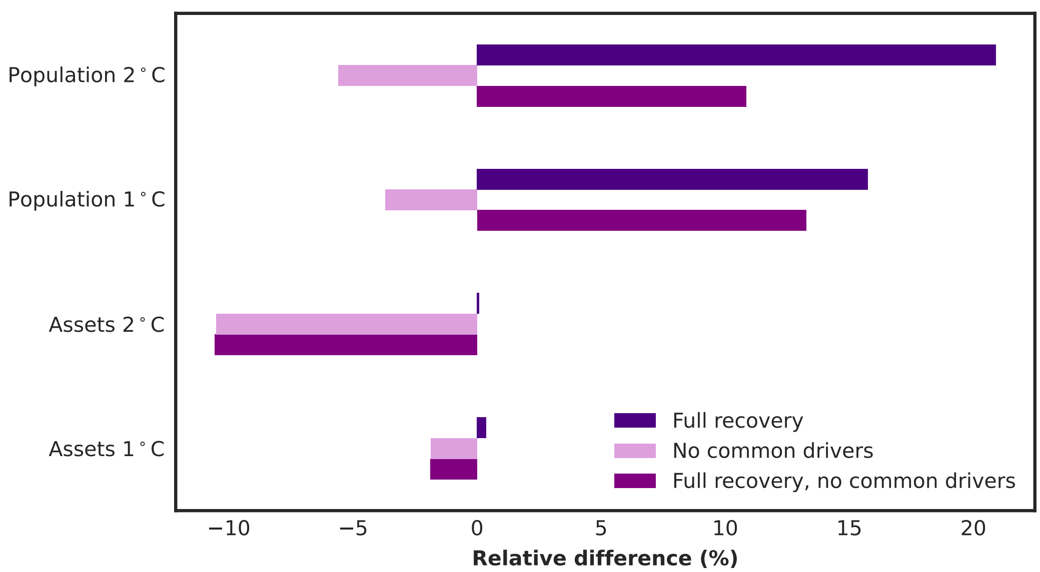

Figure 4. Relative difference in the average 100-yr impact, if common physical drivers are not considered or/and if impacts are not caped at the exposure value (assuming full recovery between single events).

Fig. 4 shows the relative difference to our estimates for the global 100-yr impact of the spatially compounding risk, when neglecting the common physical drivers or/and the recovery. Common physical drivers are considered by combining single-hazard years driven by the same GCM (see Eq. 2). We can also combine years randomly, which results in ignoring these common drivers. Recovery at the end of each year is integrated in our approach by capping the maximal impact per location k at the exposure value E_k (see Eq.2). By neglecting this condition, we can also assume full recovery in between events. For population, the relative difference shows that the impact is smaller when assuming full recovery between events. However, this assumption makes almost no difference for assets. This can be explained by the fact that assets are almost never entirely destroyed, while for population the vulnerability is binary. Neglecting common physical drivers leads to lower global impacts, especially at 2.0 °C of warming, indicating that the role of common physical drivers might be increasing with higher temperatures. Considering both physical drivers and recovery, our methods results overall in a lower risk for population, and a higher risk for assets compared to neglecting physical drivers and recovery. In the case of spatio-temporally compounding risk (See SI section 2), combining years based on the same GCMs results in lower impacts at the same return periods compared to combining random years. This indicates that common drivers may decrease the occurrence of TC and RF at the same exposure points, emphasizing that the effect of those may differ for local multi-hazard risk assessments.

Effect of climate change

In Fig. 5, we compare the spatially compounding risk curves for the present level of global warming (1.0 °C), from Fig. 3, with risk curves for further warming (2.0 °C). Only the change in climate is considered here, and we do not project socio-economic development. When comparing these two warming levels, the mean 100-yr impact increases by 13% for assets (Fig. 5 a) and by 22% for affected population (Fig. 5 b) in a 2.0 °C world. Moreover, Table 1 shows the contribution of the single hazards to this increase in combined impacts for the two studied exposures (see SI section 1 for the impact return period curves of the single hazard risks). It illustrates that the contribution of RF are more pronounced, in particular regarding increases in affected population under climate change. The increase in TC risks is more clearly observed for population, once more due to the definition of vulnerabilities. Table 1 additionally shows the relative change of the spatio-temporally compounding risks. Both the AAI and 100-yr impact increase more than for the spatially compounding risks, and in the case of assets, more than for the single-hazards (See SI section 3 for the risk curves).

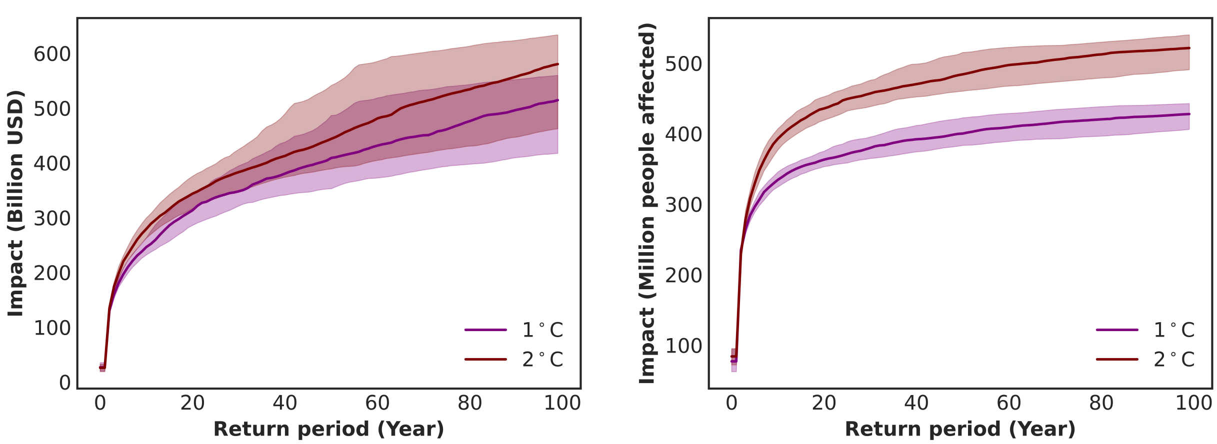

(a) Impact return period curve for assets

(b) Impact return period curve for population

Figure 5. Impact return period curves of assets (a) and population (b) being affected by both RF and TC at 1.0 °C and 2.0 °C global warming. The shaded area represents the 90th confidence interval for 1000 samples of 500 years, while the full lines represent the mean of the samples. Changes in exposure are not considered.

Table 1. Relative changes in impacts between 1.0 °C and 2.0 °C in global warming for the two risk metrics 100-yr impacts and AAI affecting the two exposures assets and population

Risk metric		Assets	Population
100-yr impact	Spatio-temporally compounding	28%	24%
	Spatially compounding	13%	22%
	Single-hazards	TC 10% | RF 11%	TC 20% | RF 28%
AAI	Spatio-temporally compounding	29%	28%
	Spatially compounding	11%	20%
	Single-hazards	TC 2% | RF 12%	TC 15% | RF 21%

Discussion

In this study, we developed a novel framework to assess multi-hazard risk for present and future climate conditions in a globally consistent way. This framework differs radically from the most naive approach consisting in assessing risks for each hazard individually and deciding on adaptation or risk transfer options for each hazard separately. The latter occurs for instance when developing separate insurance products for two independent hazards. This then results in total reserves designed to buffer the sum of both risk (e.g., of the 100-yr impacts) which are likely to overestimate the actual need. Indeed, it is highly unlikely that both 100-yr impacts occur in the same year. For independent hazards, the estimation of the 100-yr spatially compounding impacts can be improved by computing the shared exceedance probability of losses by considering the impacts of all events of both hazards, ignoring which one caused the impact[4]. However, this approach is unsuited to assess risks when the hazards are strongly correlated, for instance, due to common physical drivers. Our framework addresses this issue by accounting for these common physical drivers consistently and across climate projections. Interestingly, in the example of TCs and RFs studied in this work, including common physical drivers in the risk assessment led to higher global risk compared to considering the hazards to be independent.

Furthermore, our framework allows to include assumptions on recovery. Indeed, the use of impact time series allows the inclusion of recovery of the vulnerability and exposure over time. In the RF and TC example presented here, we considered the limiting case that vulnerability remains unchanged and that exposures has 100% recovery after each calendar year, but no recovery within the year. This assumption is reasonable for the affected population, such as those who have been displaced, and for low-impact on physical assets, such as shattered windows that can be replaced quickly. However, it may not be optimal for stronger impacts, that may lead to the reconstruction of collapsed buildings, which likely takes longer and result in increased vulnerability during the rebuilding process. This assumptions led to lower overall risks when compared to the case when no recovery was included, especially in the case of population. Note that this is mainly due to the fact that we did not include recovery within a given year (thus, the maximum impact for all RF and TC events combined within a given year is at each location maximally equal to the value of the exposure at this location).

Hence, including recovery information as well as combining hazard with common physical drivers consistently gives rise to complex interactions with non-trivial consequences for the overall risk assessment. In our example, when considering both physical drivers and recovery, we obtained lower overall risks for population, and higher overall risks for assets compared to neglecting both factors.

Beyond the inclusion of recovery and common drivers, our framework allows studying consistently the risk of multi-hazards over custom spatio-temporal scales. For instance, in our example, we looked at the impact of either TC, RF or both at each exposure location on a $150''$ resolution in a given year. Hence, one can study individual years, which can be useful in the development of storylines[18], for instance by selecting an extreme spatio-temporally compounding year with particularly many exposures impacted by both RF and TC. We further considered the average annual risk of either TC, RF or both at each exposure point, which allows to identify regions that are particularly at multi-hazard (TC and RF) risk, as well as regions that are at risk of either or.

The presented framework contains all the elements required to perform a complete multi-risk assessment. With the example shown here, we focused mainly on the multi-hazard aspects and considered a simplified description of exposures and vulnerabilities with regard to the multi-risk framework. A more in-depth analysis should improve on these components. In our study, we used regionally calibrated impact functions for the assets, but only one global step function for the affected population due to a lack of better information available in the literature. This difference in vulnerability definition played a central role in the results obtained. Additionally, our assumptions on recovery were kept simple and only applied to the exposure component of the risk. However, one should recognize that vulnerabilities may also be affected in the recovery process. For example, buildings or people that have been affected by a hazard event may be more vulnerable to a subsequent event (of the same hazard or of another) if they didn't have sufficient time to recover[12]. In order to perform a full multi-risk assessment, exposure, and vulnerabilities must therefore both also be time-dependent[3] to reflect the complexity of recovery. In most cases, the data availability and the complexity of the recovery process in a multi-hazard setting will probably hinder the use of hyper-detailed models, and thus modellers will have to choose the appropriate level of detail for their study. The same applies to hazard interactions, where other interactions than physical drivers could be incorporated. The here presented framework has the advantage of both accommodating simple component models and more complex ones, which makes it suitable for multi-risk analysis with incremental complexity.

While the presented results have a strong multi-hazard modelling approach, it is important to also acknowledge the limitation thereof. The estimates of TC impacts are based on the wind hazard as a proxy for all damages from TCs combined and do not account for the effects of TC flooding due to storm surge and torrential rainfall[19]. While we argue that considering wind as a proxy for all damages is a good approximation for a global assessment to account for yearly compounding risks, for higher time or space resolutions it would beneficial to consider the compound risks due to these sub-hazards. These could for instance be integrated in this framework by defining the spatially compounding risks by hour or days rather than by years. Note that even for global risk assessment using the wind hazard as a proxy has limitations in particular in a changing climate as TC wind and flood sub-hazards are expected to change differently[20,21]. Regarding RF, our results are limited by the modelling performance of the ISIMIP2 flood modelling cascade. Flooded areas and impacts derived with a similar method, but with observational climate forcing have shown to reproduce satellite observed flooded areas with regionally varying accuracy, depending also on the choice of the global hydrological model and the climate forcing[22]. Sources of uncertainties associated with the translation of the climate forcing into discharge refer to the exact timing and scaling of peak-runoff[23,24] and the translation into spatially explicit flood-depth on the basis of Digital Elevation Models[25]. The exact representation of flooded areas may particularly depend on the adequate representation of flood protection levels. In this study, present flood protection standards are implemented coarsely by means of the FLOPROS[26]. Previous studies suggest that these protection standards alongside the continental depth-damage functions[27] may lead to an underestimation of damage in high-income areas and an overestimation in low-income world regions[22].

Further analysis should investigate other climate risks such as heatwaves, wildfires, and droughts, for which considering common physical drivers may be central as these can be strongly correlated. To this end, efforts such as ISIMIP providing consistent models across various hazards are crucial[28]. A limiting factor is that these models are not designed to generate large probabilistic event sets, which renders the study of tail risks challenging. For example the case of RF in this work, the number of years was limited to the number of combinations of GCM years and hydrological models. Additionally, only the maximum annual flood depth is provided with ISIMIP, limiting the event-based approach. The coverage of extreme events could be improved by modelling large samples of hydro-meteorological events consistent with the physics of the GCMs, for example using coupled statistical-dynamical models, as was possible here for TCs. These models can help us in the study of tail risks, while avoiding running expensive GCM simulations. For instance, the drivers that were considered here through the use of statistical-dynamical TC models are the ENSO phase and the Global Mean Surface Temperature (GMST), two important factors to describe global climate conditions and which have been shown to modulate both TC and RF[29,30]. Further drivers could also be considered, depending on their relevance to the studied risks and spatio-temporal scale.

After evaluating the risk associated with two different hazards, it is worth noting that this framework can also be utilized to assess the risks resulting from three or more hazards. For spatially compounding risks, it will usually be necessary to consider the total aggregated risk due to all hazards. For spatio-temporal compounding risks, assessing pairs of risks is commonly done, but assessing risks resulting from three or more hazards may also be relevant[31]. Especially when assessing compounding risks occurring over a longer period or at a larger scale, the framework can be extended to assess the risk of three or more hazards occurring simultaneously. This could be common for example for multiple hazards compounding within a year in a country.

In summary, our study represents a significant contribution towards a more holistic approach to risk modelling, emphasizing the significance of a multi-hazard perspective in uncovering the potential consequences of common physical drivers on climate risks. We provide a framework to assess the effects of climate change on multi-hazard risk on a relevant spatio-temporal scale, and to study individual events, which can also serve in the development of multi-hazard storylines. Our framework further opens the door for multi-risk modelling that considers the evolving dependencies among multiple hazards, recovery processes, and changing vulnerabilities over time, ultimately enabling more effective risk management strategies in the face of changing socio-economic and climate conditions.

Methods

In the present section, we describe how both TC and RF are modeled at $1.0\,^{\circ}$C and $2.0\,^{\circ}$C, and how we calculate their risk considering exposure and vulnerability. We furthermore describe how we combine individually modeled impacts to assess the combined risk of TC and RF.

Tropical cyclone hazard The TC hazard in CLIMADA consists of TC track sets, which are coupled with a parametric wind model to simulate a 2D wind field. In this work, we use the ISIMIP archive TC tracks generated by a statistical-dynamical TC model downscaled for four global climate models (GCMs) from the Coupled Model Intercomparison Project Phase 5 (CMIP5) archive (HadGEM2-ES, MIROC5, IPSL-CM5A-LR and GFDL-ESM2M) for RCP2.6 and RCP6.0 warming scenarios[32]. The parametric wind model implemented in CLIMADA computes the gridded 1-minute sustained winds at 10 meters above ground following Holland (2008)[33]. TC wind fields are modelled on a global spatial grid at 360″ x 360″ resolution based on Geiger et al. (2021)[34]. Geiger et al. (2021)[34] additionally developed an emulator which derives a functional dependence between the simulated TC landfall time series of each GCM and global mean surface temperature (GMST) and ENSO. This emulator can be used to draw random samples from the entire TC event set (of all GCMs) to produce larger sets of TCs for each GCM, replicating the expected number of TC landfalls and mean landfall intensity in a given region and year considering ENSO and GMST (for details see Geiger et al. (2021)[34]). We emulate two set of TCs, for two warming levels since pre-industrial time: 1.0 °C and 2.0 °C degrees of warming. We define the years corresponding to a warming level based on the 31 year running mean as reported by ISIMIP, considering 10 years above and below that level for each warming level[35] (See SI Section 4.2 for more information on the binning of years). For each of the four GCMs and two warming levels, we emulate 25 samples, which coupled with the unique GCM years, results in approximately 2500 years of TC activity.

River flood hazard As for RF, we derive spatially explicit global maps of projected flooded areas and flood depth at a 150″ resolution based on the CLIMADA implementation, including data of the ISIMIP2 derived output from the simulation rounds a[22] and b[36]. The applied dataset includes the harmonized multi-model simulations of the six global gridded global hydrological models (GHMs) participating in ISIMIP2b for the scenarios RCP 2.6, RCP 6.0 and RCP 8.5. In this study, we only incude RCP2.6 and RCP6.0 to be coherent with the TC modelling. For those, the same GCMs as for the TC modelling procedure are available. For the hazard modelling, assumed are constant socio-economic conditions from 2005 regarding e.g., urbanisation patterns, river engineering and water withdrawal. The global annual flood maps were generated following the methodology previously applied in Willner et al. (2018)[37]: The runoff output of the GHMs is first harmonized with respect to the routing scheme using the river routing model CaMa-Flood (version 3.6.2) yielding daily river discharge at 15 arcmin resolution. For each grid-cell, we select the annual maximum daily discharge and fit a generalized extreme value distribution using L-moment estimators of the distribution parameters allowing for a model bias correction of each simulation GCM/GHM combination, following the approach by Hirabayashi et al. (2013)[38]. We map the return period of each event to the corresponding flood depth in a MATSIRO model run driven by observed climate forcings, which has been shown to be consistent with observation-based data[39] providing flood depth at a 15 arcmin resolution. For the mapping, we take into account flood protection levels given in the "Merged layer" of the FLOPROS database[26], applying a threshold procedure implying that, when the protection level is exceeded, the flood occurs as if there was no initial protection; below the threshold no flooding takes place. For the final assessment, we re-aggregate the high-resolution flood depth data from 0.3’ to a 2.5’ resolution (5 km × 5 km) by retaining the maximum flood depth as well as the flooded area fraction, defined as the fraction of all underlying high-resolution grid cells where the flood depth was greater than zero. In this case, we define events as the yearly maximum flood depth at each grid point, for each year and GCM/GHM combination. We then consider the same warming levels as we did with TC, which results in approximately 600 unique years of global RF per level. This means the RF events are represented by a smaller sample than TC events.

Exposures We model population and physical asset stock values at a 150″ x 150″ resolution through the LitPop module in CLIMADA. This module provides a globally consistent methodology to disaggregate asset value data proportional to a combination of nightlight intensity and geographical population data[40]. In the case of assets, 26 countries and areas cannot be calculated to lack of data. For population, it makes use of the Gridded Population of the World datasets[41]. Both exposures are kept constant at 2018 values.

Vulnerability Vulnerability of assets to TC are modelled based on the regionally calibrated impact functions provided in CLIMADA[19]. In the case of RF, we use the global flood depth impact functions developed by the Joint Research Center of the European commission[27]. In order to estimate the population affected, a step function is defined. The threshold for RFs is set to a flood depth of 1m as done by[42]. In the case of TC, we set the threshold to 33/s or a category 1 hurricane as done by Geiger et al. (2021)[34]. For examples of vulnerability functions, see SI section 4.1.

Impact calculation Single hazard impacts are calculated by combining hazard, exposure and vulnerability, using the CLIMADA impact module[17], resulting in 4 different impact models (for the population and assets exposures, as well as for the two hazards). In case of the RF impacts to assets, we normalize the expected annual impact based based on the EM-DAT database annual average impacts from 1980-2010 in 2018 inflation adjusted value (See SI section 4.3). This is done in order to obtain a realistic ratio between both hazards. But it should be noted that the observed impacts may be underestimating the total impacts, as impacts may not always be reported. In the EM-DAT database[13], we filter for both disaster sub types "Tropical

cyclone" and "Riverine flood". We then compare these values to the ones for historical period impacts. In order to account for the growth in the total asset affected value, we normalize the historical observed impacts based on the global GDB of 2018. The ratio of historical average annual impact over the modelled one is then multiplied with historical and future impacts.
For TC, we first calculate impacts on an event basis, with each event corresponding to a track. For both TC and RF, each event has a tag referring to the year and the GCM driving that event.

References

1. IPCC. Climate Change 2022: Impacts, Adaptation, and Vulnerability. Contribution of Working Group II to the Sixth Assessment Report of the Intergovernmental Panel on Climate Change (2022).
2. Ward, P. J. *et al.* Review article: Natural hazard risk assessments at the global scale. *Nat. Hazards Earth Syst. Sci.* **20**, 1069–1096, DOI: 10.5194/nhess-20-1069-2020 (2020). Publisher: Copernicus GmbH.
3. Zschau, J. Where are we with multihazards, multirisks assessment capacities? Tech. Rep., European Union, Brussels, Belgium (2017). Publisher: European Union.
4. Fleming, K. *et al.* Harmonizing and comparing single-type natural hazard risk estimations. *Annals geophysics = Annali di geofisica* **59**, DOI: 10.4401/ag-6987 (2016).
5. Ward, P. J. *et al.* Invited perspectives: A research agenda towards disaster risk management pathways in multi-(hazard-)risk assessment. *Nat. Hazards Earth Syst. Sci.* **22**, 1487–1497, DOI: 10.5194/nhess-22-1487-2022 (2022).
6. Gallina, V. *et al.* A review of multi-risk methodologies for natural hazards: Consequences and challenges for a climate change impact assessment. *J. Environ. Manag.* **168**, 123–132, DOI: 10.1016/j.jenvman.2015.11.011 (2016).
7. Gill, J. C. *et al.* Handbook of Multi-Hazard, Multi-Risk Definitions and Concepts. Tech. Rep. (2022). DOI: 10.5281/zenodo.7135138. Publisher: Zenodo.
8. Gill, J. C. & Malamud, B. D. Reviewing and visualizing the interactions of natural hazards. *Rev. Geophys.* **52**, 680–722, DOI: 10.1002/2013RG000445 (2014). _eprint: https://onlinelibrary.wiley.com/doi/pdf/10.1002/2013RG000445.
9. Gill, J. C. & Malamud, B. D. Hazard interactions and interaction networks (cascades) within multi-hazard methodologies. *Earth Syst. Dyn.* **7**, 659–679, DOI: 10.5194/esd-7-659-2016 (2016). Publisher: Copernicus GmbH.
10. Zscheischler, J. *et al.* Future climate risk from compound events. *Nat. Clim. Chang.* **8**, 469–477, DOI: 10.1038/s41558-018-0156-3 (2018). Number: 6 Publisher: Nature Publishing Group.
11. Hillier, J. K., Matthews, T., Wilby, R. L. & Murphy, C. Multi-hazard dependencies can increase or decrease risk. *Nat. Clim. Chang.* **10**, 595–598, DOI: 10.1038/s41558-020-0832-y (2020). Number: 7 Publisher: Nature Publishing Group.
12. de Ruiter, M. C. *et al.* Why We Can No Longer Ignore Consecutive Disasters. *Earth's Futur.* **8**, e2019EF001425, DOI: 10.1029/2019EF001425 (2020). _eprint: https://onlinelibrary.wiley.com/doi/pdf/10.1029/2019EF001425.
13. EM-DAT | The international disasters database.
14. Warszawski, L. *et al.* The Inter-Sectoral Impact Model Intercomparison Project (ISI–MIP): Project framework. *Proc. Natl. Acad. Sci.* **111**, 3228–3232, DOI: 10.1073/pnas.1312330110 (2014). Publisher: Proceedings of the National Academy of Sciences.
15. Golnaraghi, M. Managing Physical Climate Risk: Leveraging Innovations in Catastrophe Risk Modelling. Tech. Rep. (2018).
16. Masson-Delmotte, V. *et al.* (eds.) *Climate Change 2021: The Physical Science Basis. Contribution of Working Group I to the Sixth Assessment Report of the Intergovernmental Panel on Climate Change* (Cambridge University Press, Cambridge, United Kingdom and New York, NY, USA, 2021).
17. Aznar-Siguan, G. & Bresch, D. N. CLIMADA v1: a global weather and climate risk assessment platform. *Geosci. Model. Dev.* **12**, 3085–3097, DOI: 10.5194/gmd-12-3085-2019 (2019). Publisher: Copernicus GmbH.
18. Shepherd, T. G. *et al.* Storylines: an alternative approach to representing uncertainty in physical aspects of climate change. *Clim. Chang.* **151**, 555–571, DOI: 10.1007/s10584-018-2317-9 (2018).
19. Eberenz, S., Lüthi, S. & Bresch, D. N. Regional tropical cyclone impact functions for globally consistent risk assessments. *Nat. Hazards Earth Syst. Sci.* **21**, 393–415, DOI: 10.5194/nhess-21-393-2021 (2021). Publisher: Copernicus GmbH.
20. Knutson, T. *et al.* Tropical Cyclones and Climate Change Assessment: Part II: Projected Response to Anthropogenic Warming. *Bull. Am. Meteorol. Soc.* **101**, E303–E322, DOI: 10.1175/BAMS-D-18-0194.1 (2020). Publisher: American Meteorological Society Section: Bulletin of the American Meteorological Society.

21. Emanuel, K. Assessing the present and future probability of Hurricane Harvey's rainfall. *Proc. Natl. Acad. Sci.* **114**, 12681–12684, DOI: 10.1073/pnas.1716222114 (2017). Publisher: Proceedings of the National Academy of Sciences.

22. Sauer, I. J. *et al.* Climate signals in river flood damages emerge under sound regional disaggregation. *Nat. Commun.* **12**, 2128, DOI: 10.1038/s41467-021-22153-9 (2021).

23. Beck, H. E. *et al.* Global evaluation of runoff from 10 state-of-the-art hydrological models. *Hydrol. Earth Syst. Sci.* **21**, 2881–2903, DOI: 10.5194/hess-21-2881-2017 (2017). Publisher: Copernicus GmbH.

24. Zaherpour, J. *et al.* Worldwide evaluation of mean and extreme runoff from six global-scale hydrological models that account for human impacts. *Environ. Res. Lett.* **13**, 065015, DOI: 10.1088/1748-9326/aac547 (2018). Publisher: IOP Publishing.

25. Yamazaki, D., Kanae, S., Kim, H. & Oki, T. A physically based description of floodplain inundation dynamics in a global river routing model. *Water Resour. Res.* **47**, W04501, DOI: 10.1029/2010WR009726 (2011). ADS Bibcode: 2011WRR....47.4501Y.

26. Scussolini, P. *et al.* FLOPROS: an evolving global database of flood protection standards. *Nat. Hazards Earth Syst. Sci.* **16**, 1049–1061, DOI: 10.5194/nhess-16-1049-2016 (2016). Publisher: Copernicus GmbH.

27. Huizinga, J., Moel, H. d. & Szewczyk, W. Global flood depth-damage functions: Methodology and the database with guidelines. *JRC Res. Reports* (2017). Number: JRC105688 Publisher: Joint Research Centre (Seville site).

28. Frieler, K. *et al.* Assessing the impacts of 1.5 °C global warming – simulation protocol of the Inter-Sectoral Impact Model Intercomparison Project (ISIMIP2b). *Geosci. Model. Dev.* **10**, 4321–4345, DOI: 10.5194/gmd-10-4321-2017 (2017). Publisher: Copernicus GmbH.

29. Sabbatelli, T. A. & Mann, M. E. The influence of climate state variables on Atlantic Tropical Cyclone occurrence rates. *J. Geophys. Res. Atmospheres* **112**, DOI: 10.1029/2007JD008385 (2007). _eprint: https://onlinelibrary.wiley.com/doi/pdf/10.1029/2007JD008385.

30. Ward, P. J. *et al.* Strong influence of El Niño Southern Oscillation on flood risk around the world. *Proc. Natl. Acad. Sci.* **111**, 15659–15664, DOI: 10.1073/pnas.1409822111 (2014). Publisher: Proceedings of the National Academy of Sciences.

31. Claassen, J. N. *et al.* MYRIAD-HESA: A New Method to Generate Global Multi-Hazard Event Sets. preprint, In Review (2023). DOI: 10.21203/rs.3.rs-2635188/v1.

32. Emanuel, K. A. Downscaling CMIP5 climate models shows increased tropical cyclone activity over the 21st century. *Proc. Natl. Acad. Sci.* **110**, 12219–12224, DOI: 10.1073/pnas.1301293110 (2013).

33. Holland, G. A Revised Hurricane Pressure–Wind Model. *Mon. Weather. Rev.* **136**, 3432–3445, DOI: 10.1175/2008MWR2395.1 (2008). Publisher: American Meteorological Society Section: Monthly Weather Review.

34. Geiger, T., Gütschow, J., Bresch, D. N., Emanuel, K. & Frieler, K. Double benefit of limiting global warming for tropical cyclone exposure. *Nat. Clim. Chang.* **11**, 861–866, DOI: 10.1038/s41558-021-01157-9 (2021). Number: 10 Publisher: Nature Publishing Group.

35. ISIMIP. ISIMIP2b temperature thresholds and time slices (2017).

36. Bertram, C. *et al.* NGFS Climate Scenario Database: Technical Documentation V2.2 (2021). Publisher: Potsdam Institute for Climate Impact Research (PIK), International Institute for Applied Systems Analysis (IIASA), University of Maryland (UMD), Climate Analytics (CA), Swiss Federal Institute of Technology (ETHZ).

37. Willner, S. N., Levermann, A., Zhao, F. & Frieler, K. Adaptation required to preserve future high-end river flood risk at present levels. *Sci. Adv.* **4**, eaao1914, DOI: 10.1126/sciadv.aao1914 (2018).

38. Hirabayashi, Y. *et al.* Global flood risk under climate change. *Nat. Clim. Chang.* **3**, 816–821, DOI: 10.1038/nclimate1911 (2013). Number: 9 Publisher: Nature Publishing Group.

39. Kim, H., Yeh, P. J.-F., Oki, T. & Kanae, S. Role of rivers in the seasonal variations of terrestrial water storage over global basins. *Geophys. Res. Lett.* **36**, DOI: 10.1029/2009GL039006 (2009). _eprint: https://onlinelibrary.wiley.com/doi/pdf/10.1029/2009GL039006.

40. Eberenz, S., Stocker, D., Röösli, T. & Bresch, D. N. Asset exposure data for global physical risk assessment. *Earth Syst. Sci. Data* **12**, 817–833, DOI: 10.5194/essd-12-817-2020 (2020).

41. Gridded Population of the World (GPW), v4 | SEDAC.

42. Kam, P. M. *et al.* Global warming and population change both heighten future risk of human displacement due to river floods. *Environ. Res. Lett.* **16**, 044026, DOI: 10.1088/1748-9326/abd26c (2021). Publisher: IOP Publishing.

Acknowledgements

We are grateful to Kerry Emanuel and Marleen de Ruiter for their insightful comments and suggestions, which greatly improved the quality of our work.

This project has received funding from the European Union's Horizon 2020 research and innovation program (grant agreements No 821010 and No 820712) and from the Swiss Innovation Agency Innosuisse (project number 53733.1 IP-SBM).

Author contributions statement

Z.S., C.B.S., C.M.K. and D.N.B. developed the methodology. T.V. developed the TC emulator, S.M. and I.J.S. provided the hazard data and data description in the manuscript, Z.S. conducted the analysis, analysed the results and generated the figures, Z.S., C.B.S. and C.M.K. wrote the manuscript. All authors reviewed and edited the manuscript.

Additional information

Competing interest statement The authors declare no competing interests.

Data availability

The TC track simulations are available for scientific purposes only and upon request from WindRiskTech (info@windrisktech.com). The ISIMP data to generate RF is available at `https://zenodo.org/record/4627841#.Y_nyRy8w1hH`. The population and asset data is available through the CLIMADA data API `https://climada.ethz.ch/data-api/v2/docs`. EM-DAT historical damages are available at `https://public.emdat.be/`.

Code availability

The simulations to quantify the TC impact were conducted using the Python tool CLIMADA, available at `https://github.com/CLIMADA-project/climada_python/` (a frozen version was made available at https://doi.org/10.5281/zenodo.6807463). In particular, the tool to generate the artificial TC exposure time series is freely available at `https://github.com/CLIMADA-project/climada_petals/blob/main/doc/tutorial/climada_hazard_emulator.ipynb`. The scripts used in this work will be made available.

Supplementary information to: Global multi-hazard risk assessment under climate change

1 Effect of climate change on single-hazard risks

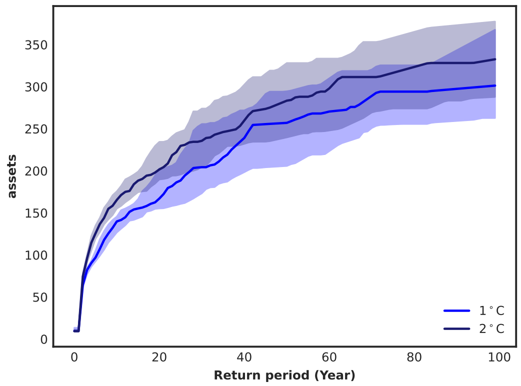

(a) Impact return period curves of RF on assets

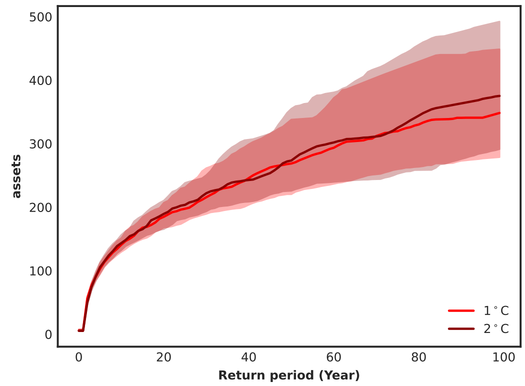

(b) Impact return period curves of TC on assets

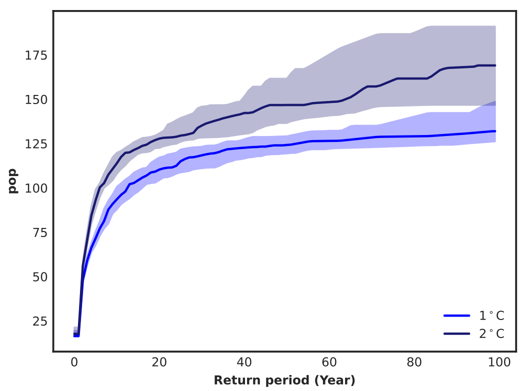

(c) Impact return period curves of RF on population

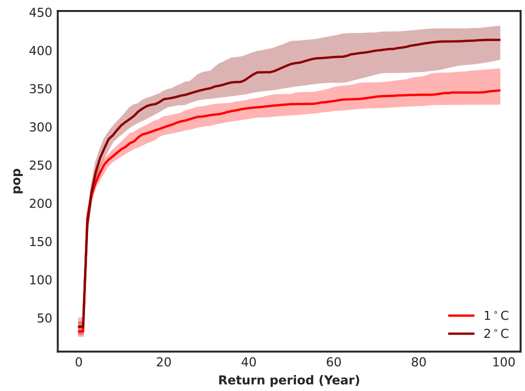

(d) Impact return period curves of TC on population

Supplementary Figure 1. Impact return period curves of single hazard impacts at 1 °C and 2 °C of warming

2 Effect of common physical drivers on compound risks

For both levels of warming, the median curves of combined impacts appears to always be equal or higher when considering common physical drivers (see Suppl. Fig. 2).

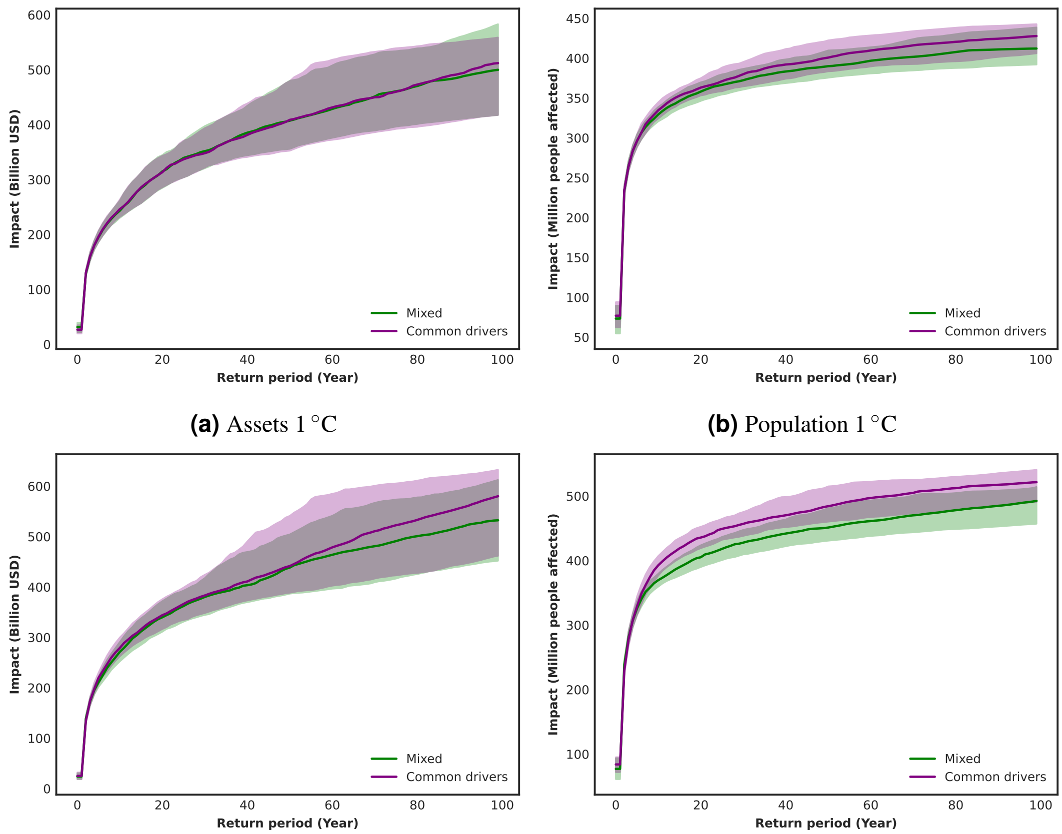

(a) Assets 1 °C

(b) Population 1 °C

(c) Assets 2 °C

(d) Population 2 °C

Supplementary Figure 2. Spatially compounding impact return period curves of combined impacts, when considering common physical drivers or randomly mixing years

3 Effect of climate change on spatio-temporally compounding impact return period curves

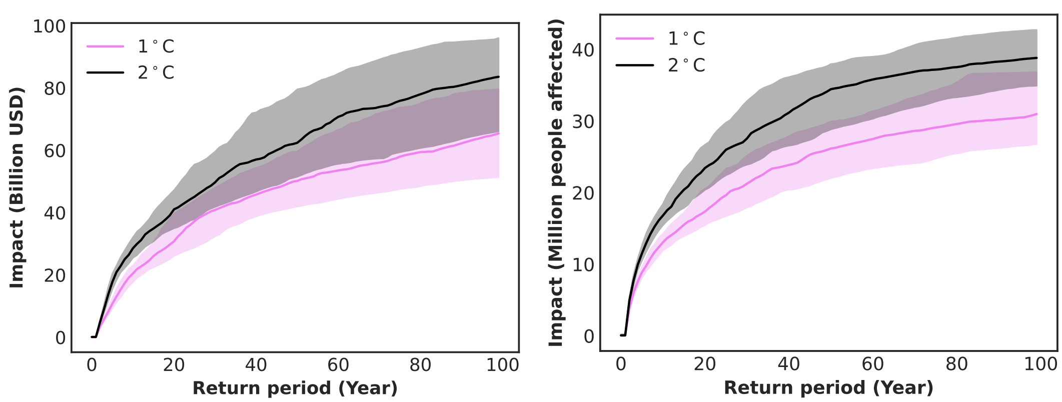

(a) assets

(b) population

Supplementary Figure 4. Compound impact return period curves at 1 °C and 2 °C

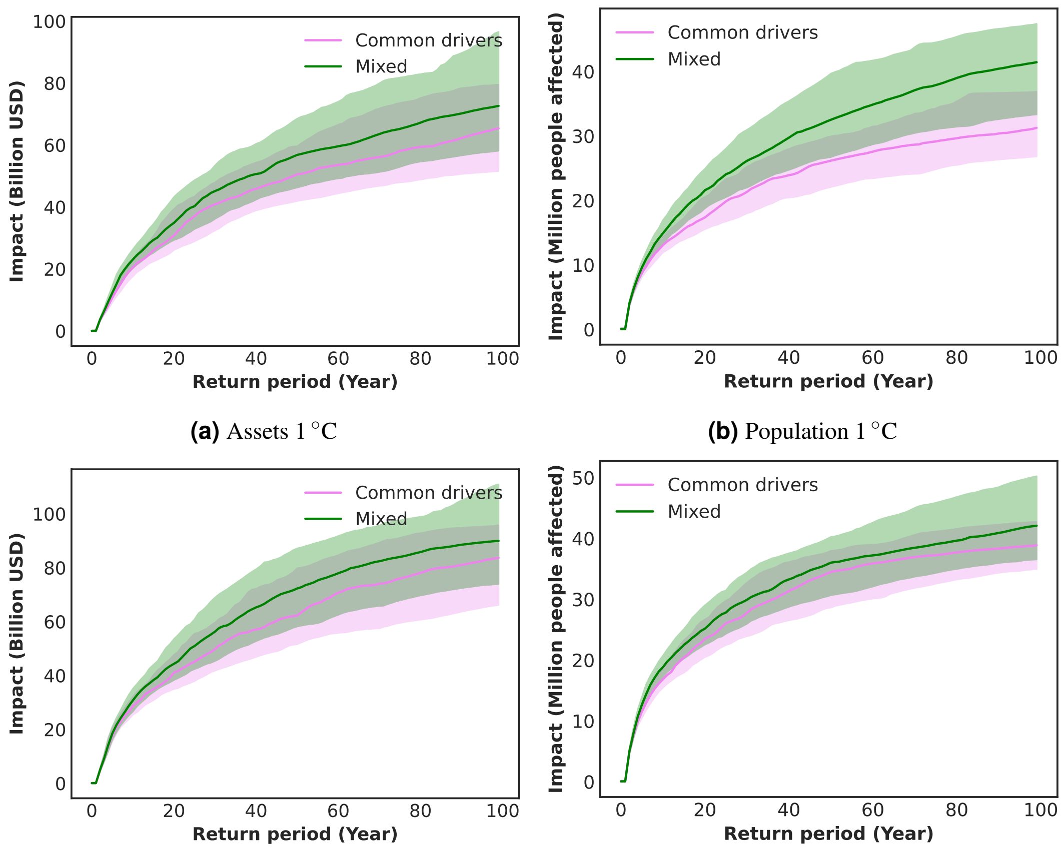

(a) Assets 1 °C

(b) Population 1 °C

(c) Assets 2 °C

(d) Population 2 °C

Supplementary Figure 3. Compound impact return period curves at 1 °C and 2 °C when considering common physical drivers or randomly mixing years

4 Supplementary methods

4.1 Vulnerabilities

In Fig. 5, examples of impact functions are shown. For assets, regional functions are defined based on Eberenz et al. (2021) for TC[1] and huizinga et al. (2017)[2] for RF. In the case of population, a step function is defined based on Kam et al. (2021) and Geiger et al. (2021)[3,4].

4.2 Warming levels

Supplementary Table 1. 21 Year bins for each GCM and RCP centered around the 31-year running mean of global mean tas reaching 1 °C or 2 °C based on ISIMIP provided values[5]. We consider +-10 years around the reported year as corresponding to that warming level. As the river flood data only starts in 2006, the full 21 years bin cannot be considered. The year bins were still taken as being centered around the warming level. This results in a total of 108 years for 1 °C, and 104 years for 2 °C.

		gfdl-esm2m	miroc5	hadgem2-es	ipsl-cm5a-lr
1 degree	RCP2.6	[2006, 2023]	[2006, 2025]	[2006, 2019]	None
	RCP6.0	[2006, 2027]	[2013, 2034]	[2006, 2023]	None
2 degree	RCP2.6	None	None	None	[2019, 2040]
	RCP6.0	[2066, 2087]	[2061, 2082]	[2040, 2061]	[2019, 2040]

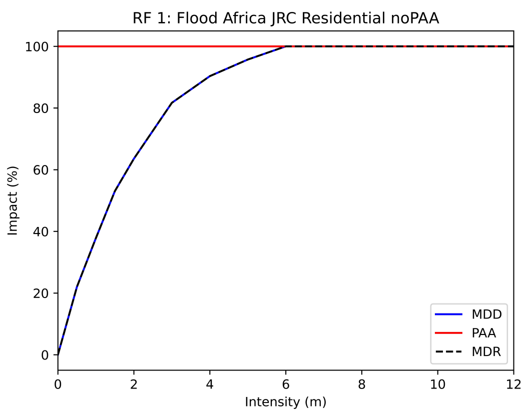

(a) RF Africa assets

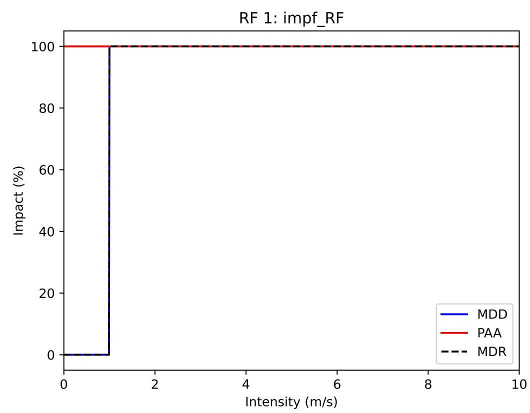

(b) RF population

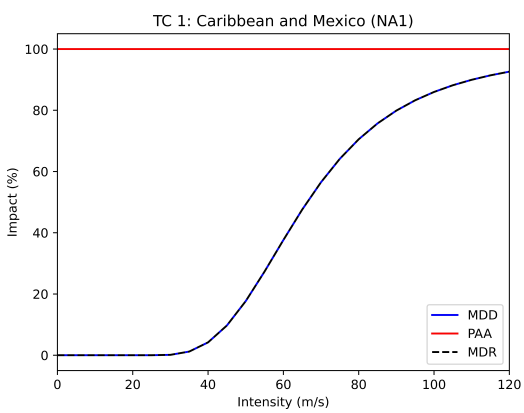

(c) TC Caribbean and Mexico assets

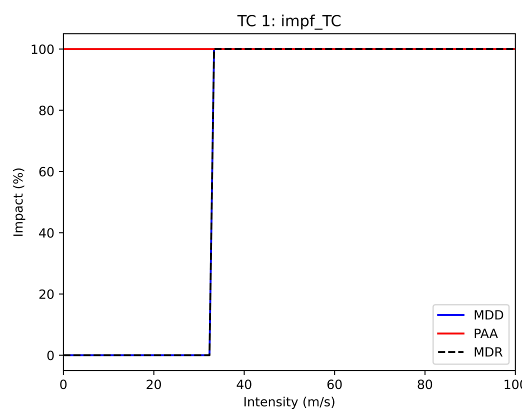

(d) TC population

Supplementary Figure 5. Example of impact functions used in the impact calculation. In the case of assets, vulnerabilities are separated in 10 regions, while for RF there are a total of 6 regions. In the case of population, one function is used per hazard with a threshold.

4.3 Normalization of river flood impacts

In the case of river flood, we obtain $ 481 Billion average annual impact (AAI) using ISIMIP2a reanalysis data for the period 1980-2010 to calculate impacts on the LitPop asset exposure used in this work. Based on EM-DAT 1980-2010 values, historical reported impacts to be $ 48 Billion AAI, when adjusting for growth based on[6] and inflation adjusted to 2018 values. This is a factor 10 higher than the calculated impacts.

The large difference can be explained on the one hand by the fact that we use the maximal flood depth per grid point, which we combine with vulnerability curves developed at the building level, in order to calculate the impact. We expect this to lead to overestimates, but still allows to account for regional differences in vulnerability. Additionally, there is a wide spread in the impacts caused by each model combination. The study by Sauer et al. (2021) considered the median of the hydrological models at a regional level before summing impacts globally, additionally removing outliers[7]. Finally the EM-DAT database only contains observed events, while historical impacts may in reality be larger.

In the case of the present studies, the focus is not on the exact values of the average impacts, but rather on extreme values. We therefore give the same weight to all the model combination by considering the mean as the average annual impact. We however normalize the river floods impacts in order to have a realistic ratio between TC and RF impacts.

References

1. Eberenz, S., Lüthi, S. & Bresch, D. N. Regional tropical cyclone impact functions for globally consistent risk assessments. *Nat. Hazards Earth Syst. Sci.* **21**, 393–415, DOI: 10.5194/nhess-21-393-2021 (2021). Publisher: Copernicus GmbH.
2. Huizinga, J., De, M. H. & Szewczyk, W. Global flood depth-damage functions: Methodology and the database with guidelines, DOI: 10.2760/16510 (2017). ISBN: 9789279677816 ISSN: 1831-9424.
3. Kam, P. M. *et al.* Global warming and population change both heighten future risk of human displacement due to river floods. *Environ. Res. Lett.* **16**, 044026, DOI: 10.1088/1748-9326/abd26c (2021). Publisher: IOP Publishing.
4. Geiger, T., Gütschow, J., Bresch, D. N., Emanuel, K. & Frieler, K. Double benefit of limiting global warming for tropical cyclone exposure. *Nat. Clim. Chang.* **11**, 861–866, DOI: 10.1038/s41558-021-01157-9 (2021). Number: 10 Publisher: Nature Publishing Group.
5. ISIMIP. ISIMIP2b temperature thresholds and time slices (2017).
6. Worldbank. GDP growth (annual %) | Data (2023).
7. Sauer, I. J. *et al.* Climate signals in river flood damages emerge under sound regional disaggregation. *Nat. Commun.* **12**, 2128, DOI: 10.1038/s41467-021-22153-9 (2021).